

## Thermal performance of double-layer porous copper strips mounted as hollow cylinders

Ahmed AAG. Alrubaiy<sup>a,\*</sup>, Basim A.R. Al-Bakri<sup>b</sup> and Radwan M. Aljuhashy<sup>c</sup>

<sup>a</sup> Department of Materials Engineering, Diyala University, Baquba, Diyala Province, Iraq

<sup>b</sup> Department of Aeronautical Engineering, University of Baghdad, Aljadriya, Baghdad, Iraq

<sup>c</sup> Department of Mechanical Engineering, Wasit University, Kut, Wasit, Iraq

---

### ABSTRACT

The thermal performance of thin double-layer porous copper strips was experimentally examined. To fabricate double-layer porous copper strips the lost carbonate sintering procedure was employed. The suitability of these materials for applications of heat sink was systematically investigated. Then, the thermal properties of an external heat transfer facility, which operates under a forced heat convection process using air as a coolant, were assessed. In this case, a cylindrical heating system was chosen to be used with the air passing across the samples at mass rates of 0.1- 0.5 kg/s. The temperatures of the air at the inlet and outlet in addition to the surface temperature of the system were monitored and used to determine the heat transfer performance. The results showed that both the porosity and roughness in a surface of a material could play an essential role in such type of material in enhancing heat transfer at a surface of the system. With high porosity and surface roughness of up to 82% and  $R_a \leq 1.21$  mm, respectively, the sample achieved a thermal transmittance 57% higher than that of a reference smooth copper sheet under the same Reynolds number. Finally, the heat transmittance of the examined porous sheets in the current research increased with the bulk porosity and surface roughness.

---

**Keywords:** Porosity; Copper sheets; Tape casting; Roughness surface heat transfer; heat sink; heat exchanger.

---

### *Corresponding Author:*

Ahmed AAG. Alrubaiy  
Department of Materials Engineering  
Diyala University, Baquba, Diyala Province, Iraq  
ghaidan3@gmail.com

---

### 1. Introduction

Very thin and porous layers of a wide surface area of a copper material to the thickness ratio are potentially attractive. This could be achieved for the thermal management in space-limited devices where better performance of heat transfer within confined dimensions is highly required. Currently, thermal aspects have been becoming increasingly important in order to ensure high performance device, when electronics has become more compact and slimmer than before. [1], [2]. A type of porous metals, which is well-known open-celled, with small thicknesses and high energy is likely to be suitable for the current application. However, other types of metals, which are made from copper in porous form, can highly conduct heat extremely. Therefore, porous copper metals have been considered in manufacturing of the body of heat exchangers and heat sinks [3-6]. Performance of heat transfer of different forms of porous material has been studied and reported, from lotus-structure types [7], [8], and [9], to open-celled structure types [4], [5], and [10]– [13]. This work has demonstrated that the performance of heat transfer of a porous material heat exchanger is mainly influenced by the porosity/density of the porous medium and the morphology of the pores and morphology of the cell walls. The heat transfer process through a porous material is controlled by conductive heat transfer within the solid, with a lesser contribution from radiative heat transfer between the cell walls. Heat transport from a heat exchanger to the flowing fluid is dominated by convective heat transfer. Therefore, the overall heat transferred

from the heat source by a porous metal heat exchanger depends on the mesostructure. The arrangement of porosity is explained as the mesostructure, which is also defined as the structural level between the metallic microstructure and the overall form of the component. The key factors that affect the volumetric porosity and pore morphology are in turn dependent on the manufacturing technology and process conditions adopted in producing the sample [3] and [14]– [17]. These may not be the only factors; surface roughness has also been shown to have a huge effect on the performance heat transfer of heat sinks [18]– [20], although this has not been specifically explored in porous metals.

In the current study, a thickness down to 1.4 mm of porous sheets of copper was manufactured and investigated for the performance of heat transfer. Moreover, the current copper samples were formed by lost carbonate sintering for the casting of copper strips [21]. This process paves the way to control both thickness and porosity of the component. The strips consisted of two porous layers with porosity in the range of 50 - 82% substrates of 0.125 mm thickness. This design was used to provide a solid backing that could be placed in contact with a component requiring cooling, and to have this backing intimately connected to a porous region within which heat transfer would take place. The thermal properties of the system will be assessed by forced heat convection using a coolant fluid (air). Temperatures of the system (fluid and structure) will be monitored by employing an open-circuit instrument of heat transfer. Additionally, smooth surfaces and non-porous copper sheets will be thoroughly investigated under similar boundary conditions to that of the provided reference case study.

## 2. Experimental approach

### 2.1 Sample preparation

Samples with double porous layers were produced by the lost carbonate sintering process. For cast copper stripes, the raw materials were dendritic powder copper Cu, as the base metal and potassium carbonate  $K_2CO_3$  as the leachable space holder. The porosity can be adjusted by adding  $K_2CO_3$  at percentage of 10 – 50 wt, as shown in Table 1. The powders were mixed with organic binders into a homogenous slurry. The slurry was tape-cast into thin layers on top of a 0.125 mm thick copper substrate in two ways, described below as two main processing paths A and B.

*Process path A:* A slurry was directly tape cast on adense copper of 0.125 mm thickness controlled using a built-in stationary blade. Under a vacuum environment conditions, the samples were obtained through debinding at 450°C and sintering at 890°C. The space holder was detached by dissolution in water at room temperature, and the porous copper sheets produced are shown in Figure 1. These samples were observed to have relatively low porosities visible from the surface.

*Process path B:* The path was developed to attempt to increase the porosity. In contrast to process path A, firstly, the slurry was a tape cast onto a non-stick silicone tape (Polyester Mylar Film), then inverted and placed onto the dense copper substrate of 0.125 mm foil. The purpose of this was to reverse the distribution of the carbonate space holder particles. It was debound and sintered under the same conditions as above. The porous samples produced by this process were observed to gain higher surface porosity compared to process path A and slightly higher volumetric porosity. The samples were produced by this path, as shown in Figure 2.

Table 1. Weight ratios of  $K_2CO_3$  and Cu used during processing of the samples

Process path	Amount of Carbonate (wt.%)				
	0P.Cu	20P.Cu	30P.Cu	40P.Cu	50P.Cu
A	0	20	30	40	50
B	0	20	30	40	50

The number refers to the added weight per cent  $K_2CO_3$ , while the middle term (P.Cu) refers to porous copper.

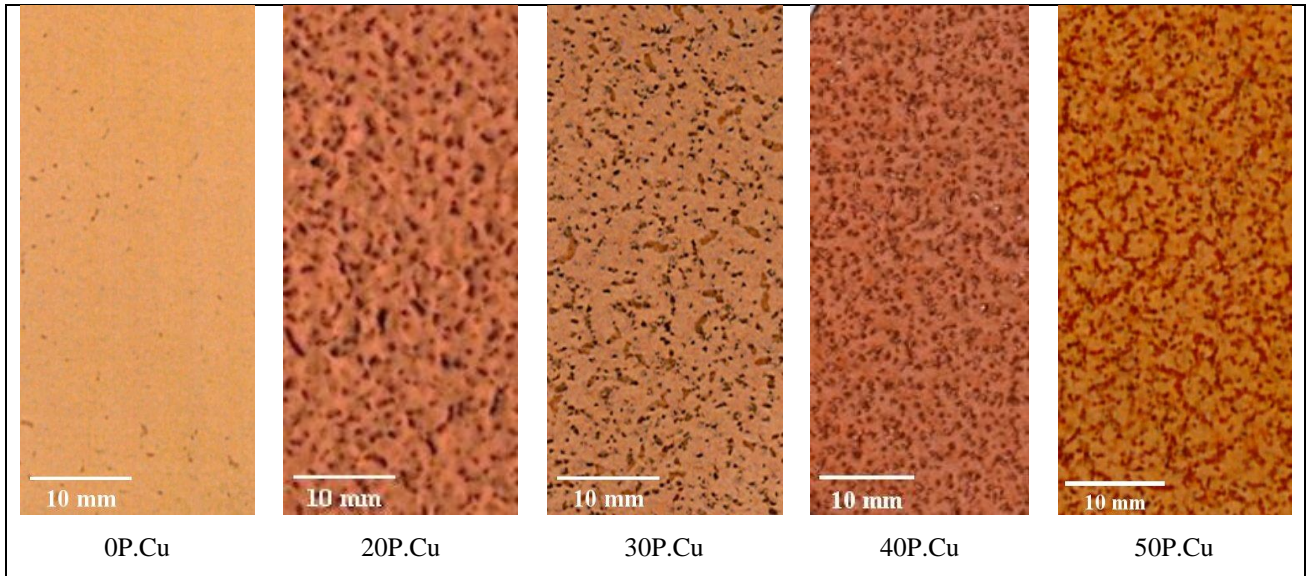


Figure 1. Strips of porous copper formed by the process path A at volumetric porosity ranges from 51% - 81%.

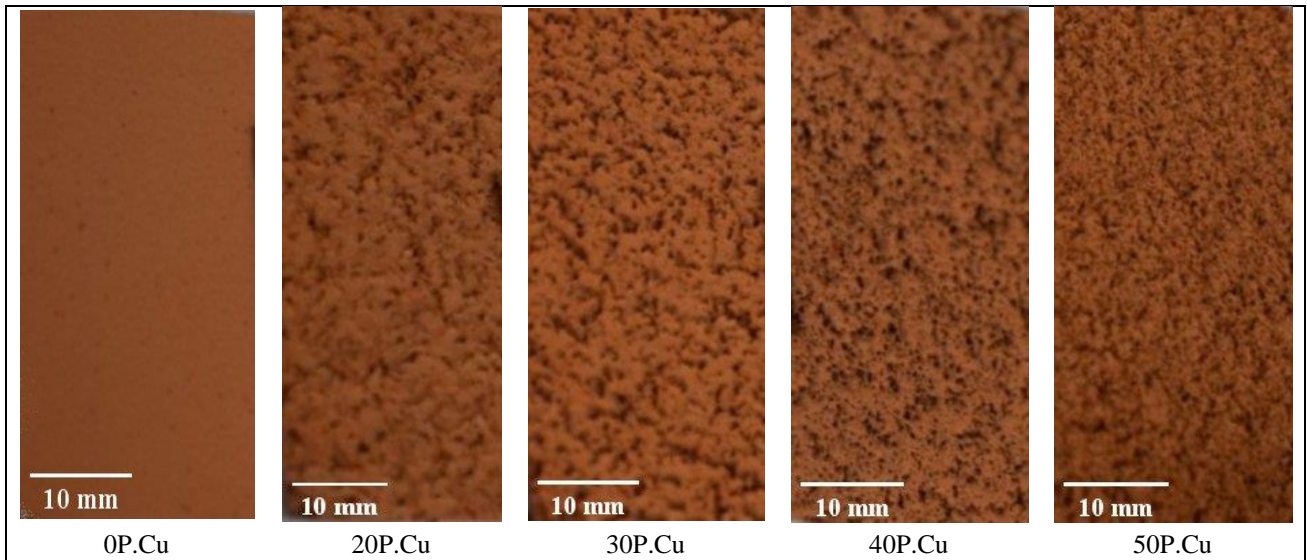


Figure 2. Strips of porous copper formed by the process path B at volumetric porosity ranges from 51% - 82%

Two sets of samples were investigated. The surface and volumetric porosity of the first set of path A ranges from 28% - 61% and 50% - 81%, respectively. The second set of path B had surface and bulk porosity that ranged from 29% - 74% and 51% - 82% respectively.

Sheet metal cutters were used to cut the sample into the required size and shape. Each sample is a double-layer thin sheet with the following dimensions of 160 mm × 100 mm × ~1.4 mm and mounted as a hollow cylinder. During processing, the sample surface developed a degree of roughness, which increased with higher additions of the carbonate space holder, and with increasing porosity.

## 2.2 Porosity and surface roughness of the samples

*Bulk porosity:* the volumetric porosity (bulk) of the porous copper sheets can be obtained by using (Accupyc 1340, Micromeritics). It is simply a helium pycnometer that depends on the following equation:

$$\varepsilon = \left(1 - \frac{\rho_a}{\rho_t}\right) \times 100 \quad (1)$$

where  $\rho_a$  refers to the apparent density, which is obtained by dividing the mass at 0.0001kg by the volume. The volume can be gained using the Vernier caliper to measure dimensions. The symbol  $\rho_t$  represents the true density of the porous surfaces that can be acquired using the helium pycnometer.

Surface porosity: The porosity of the porous copper strips was measured with the aid of actual size image analysis. Sample photographs were taken under medium to low light conditions. The reason for this was to clearly demonstrate the two different surface areas (pores and continuous) for micropores and macropores, for the sample's images. Micropores can be evaluated by SEM micrographs. The ImageJ method [22] and [23] were used for calibrating and processing the sample photographs. Any unidentified pores that appeared as dark areas on the surface were considered as surface defects, and they were removed manually. The processing was conducted in the ImageJ2 (Fiji) analysis program to calculate the cross-sectional area for each pore and their axes. The frequency of samples and K<sub>2</sub>CO<sub>3</sub> particles can be analyzed by using the Prism 9 for Macintosh OS X 10.12, GraphPad Software.

Firstly, images, which were captured by a modern technology camera (Nikon -D5200 model) built-in with 24-52 mm lens (AF-S 16-35mm f/4 G), was analyzed to study the surface roughness of the current work sheets. Secondly, Fiji software was utilized to sketch the surface shapes of samples. Then, the last step was performed the statistical analysis of these profiles by using Microsoft Excel spreadsheets.

Table 2: Results of porosity, surface area, and roughness and peak value per centimeter of porous copper strips produced and investigated in the current study for the samples of paths A and B.

Processing Path	Samples	Roughness value, $R_a$	Peaks Per Centimeter, $m$	Bulk Porosity, $\varepsilon$ (%)	Surface porosity, $P_{Surf}$ (%)	Micropores Surface Area ( $\text{cm}^2/\text{cm}^3$ )	Macropores Surface Area ( $\text{cm}^2/\text{cm}^3$ )
Path A	0P.Cu	0.031	-	50.7	28.6	2616	179
	20P.Cu	0.411	3.43	70	39.7	1693	442
	30P.Cu	0.884	4.29	75.2	45.1	1412	553
	40P.Cu	0.960	4.57	78.4	49.6	1217	641
	50P.Cu	1.209	4.86	80.5	60.5	870	833
Path B	20P.Cu	0.559	3.72	73.6	47.6	1212	621
	30P.Cu	0.841	4.29	79.0	54.6	802	799
	40P.Cu	0.957	4.57	80.4	62.1	658	920
	50P.Cu	1.030	5.43	81.5	73.4	384	1132

The porous in the current samples, which were produced from the path B process, has a high level of surface and volumetric porosity to those created from the path A, as presented in Table 2. The surface roughness of both the path A and B sheets are also summarized in Table 2. In addition, strips came from the path A have higher roughness values and number of peaks per centimeter length,  $m$  than those form the path B. Table 2 also shows the surface area of the porous in the samples considered in the current study. This clearly demonstrates the contributions of the macropores (large pores, roughly corresponding to the shape and size of particles in the space holder) and micropores (finer-scale porosity, associated with incomplete densification of the metal powder) to the total surface area of the sample.

## 2.3 Quantity of heat measurements

### 2.3.1 Experimental Setup

The suitability of the porosity in copper samples for applications that have heat transfer systems, was studied by using an open-cycle wind tunnel. Figure 3, shows a schematic diagram of the test facility which was used to study the samples. The test facility includes two centrifugal fans, hot-wire anemometer (HWA) system, wind tunnel, micro-foil heat flux sensor, and thermocouples-type, J, K, and T. Computers can run PicoLog software which acquires data. So, the function of each section of the test facility are going to be explained in the next paragraphs.

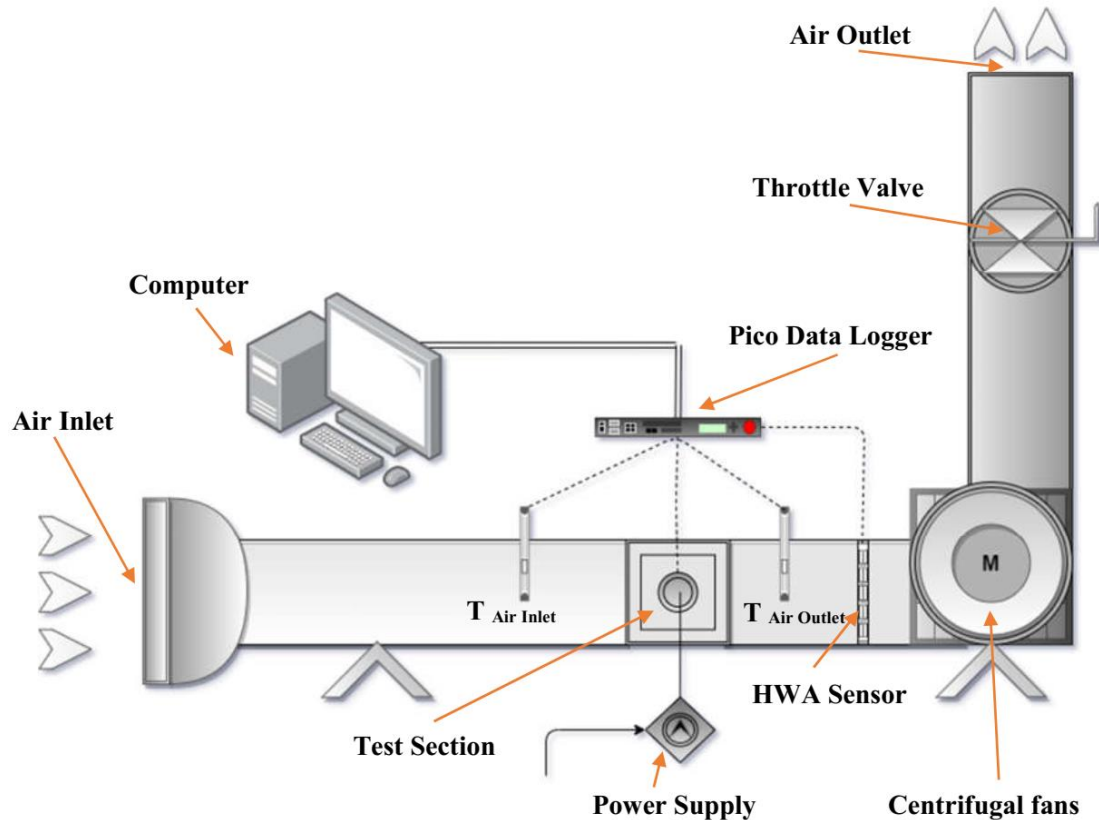


Figure 3. Schematic diagram of the thermal test facility

The two centrifugal fans, which were set at the exit of the wind tunnel as the air was forcibly introduced into the air inlet by suction. The graded throttle valves were set at the exit of the tunnel to govern the air volume. The air velocity was measured using a calibrated hot-wire anemometer (HWA). The wind tunnel consists of a square section of 125 mm. A honeycomb mesh was set up behind the test section in order to reduce the bulk flow that was induced by the centrifugal fans. Moreover, the test section was placed in the middle of the air tunnel, as seen in Figure 3. Thermocouples of K-type and T-type of up to 100  $\mu$ m was utilized to measure temperatures of the air at the inlet and outlet and the surface of the samples. These thermocouples can be logged by using PicoLog software.

The cylindrical heating system CHS, as shown in Figure 5, was specially manufactured to fit porous sheets. This system was made of an aluminum metal cylinder of 50 mm diameter, polyether ether ketone PEEK as insulator of also 50 mm diameter and a 400W cylindrical heating cartridge of 10 mm diameter, which is taken by a J-type thermocouple. The heating element was fixed at the center of the metal cylinder in order to make the homogenized heat passes in the radial direction.

The range of the velocity was between 5 m/s to 21 m/s that used to test the samples. Moreover, an RS PRO IDM66RT handheld digital multimeter, with RS calibration (AC Voltage Accuracy  $\pm 1\% + 5$  Digits) was employed to measure the power supplied to the heating element, the cartridge heater.

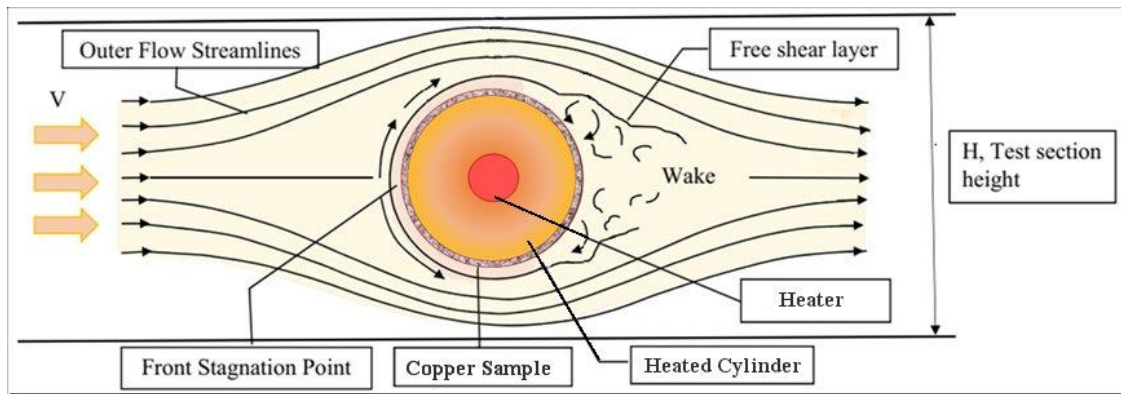


Figure 4. Schematic diagram of sample positioning and heating system relative to air duct and flow direction

### 2.3.2 Procedure of the experimental work

A metal cutter was utilized to cut a thin layer of grease (Kryonaut high thermal performance) of the current samples, which were mounted directly to the aluminum surface to ensure better thermal contact. These samples were curved around as a cylinder then the ends were joined using two - sided adhesive thin tape of up to 100  $\mu\text{m}$ . In addition, a micro foil T-type thermocouple was joined to the surface by a two-sided conductive strip of  $\square 0.1\text{mm}$ , as mentioned in Figure 5. Then the hollow sample component was set up in the test section of the air tunnel.

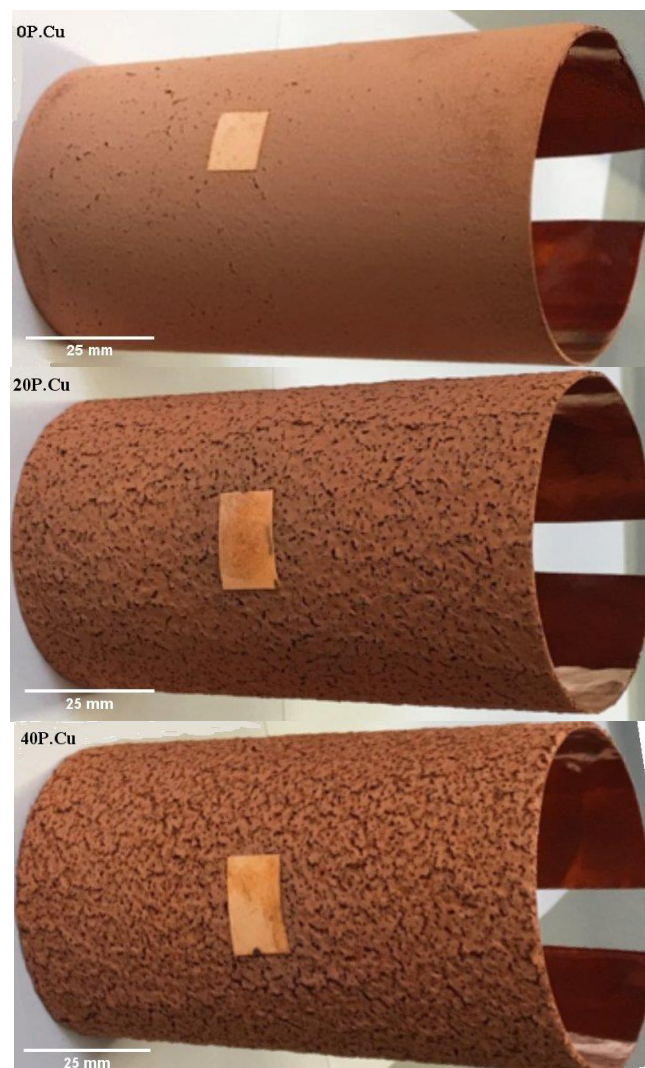


Figure 5. Tested samples mounted as hollow cylinders

When the heating system was on, the majority of the thermal energy moved through a tested sample into the atmosphere by the convection way of heat transfer  $Q_{conv}$ . Whereas, a small rate of energy passed to the barriers of the air tunnel by the conduction way  $Q_{cond}$  and radiation way  $Q_{rad}$ . Approximately 2% of the energy was found to be lost by conduction to the PEEK guards and was neglected from the analysis

$$Q_{rad} = \sigma_B \epsilon A (T_s^4 - T_t^4) \quad (2)$$

$$Q_{conv} = hA(T_s - T_a) = T_r(T_s - T_a) \quad (3)$$

$$Q_{conv} = P - Q_{rad} - Q_{cond} = P - \sigma_B \epsilon A (T_s^4 - T_t^4) \quad (4)$$

Where the constant number of Stefan-Boltzmann is represented by  $\sigma_B$  is  $5.67 \times 10^{-8} \text{ W/m}^2\text{k}^2$ ,  $\epsilon$  is the emissivity of the surface of the sample about 0.6 [25],  $T_s$  is the temperature on the surface of the sample, and  $T_t$  is the temperature of the air tunnel wall. Also,  $T_r$  is the thermal transmittance in  $\text{W/K}$  and the convective heat transfer coefficient  $h \text{ W/m}^2\text{k}$  was found as follows:

$$T_r = Q_{conv}/(T_s - T_a) = [P - \sigma_B \epsilon A (T_s^4 - T_t^4)]/(T_s - T_a), \quad (5)$$

$$h = Q_{conv}/A(T_s - T_a) = [P - \sigma_B \epsilon A (T_s^4 - T_t^4)]/A(T_s - T_a), \quad (6)$$

where  $T_a$  is the flowing air temperature  $T_a = (T_{in} + T_{out})/2$ . The Reynolds number can be expressed by the air velocity sucked inside the tunnel:

$$Re_D = uD/\nu, \quad (7)$$

where the letter  $D$  refers to the tested cylinder diameter which equals 50mm,  $\nu = 1.534 \times 10^{-5} \text{ m}^2/\text{s}$  at  $T_a = 23 \text{ C}^0$  is the air kinematic viscosity, which varies with the ambient temperature. Moreover, the average heat transfer coefficient is obtained in convection by the  $Nu$  number as follows:

$$Nu = hD/k, \quad (8)$$

where,  $k = 2.83 \times 10^{-2} \text{ W/mK}$  is the thermal conductivity of air. Properties of air in the current study, were taken according to the average temperature value of the film  $T_f = (T_s + T_a)/2$ , and also for standard atmospheric pressure.

### 3. Results and discussion

The performance of heat transfer quantity from the two paths A and B of the double-layered porous strips were examined for each sample by calculating the coefficient of thermal transmittance  $T_r$  ( $\text{W/K}^0$ ) and convection heat transfer  $h$  ( $\text{W/m K}^0$ ). Furthermore, smooth sheets without porous were verified to gain  $h$  and  $T_r$  as reference values.

The first following two plots can declare the experimental data of the performance of porous sheets of path A with varying porosity and surface roughness. Whereas, the other two plots demonstrate the results of the heat transfer effectiveness of porosity sheets of path B by varying porosity and surface roughness.

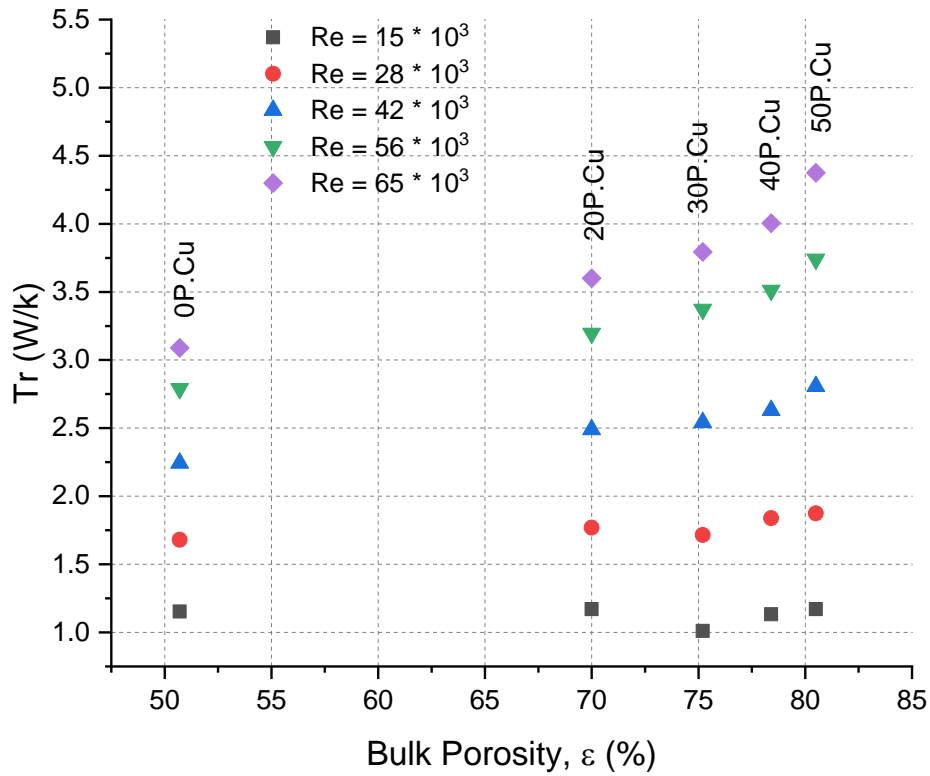


Figure 6. Thermal transmittance of path A against bulk porosity of porous sheets at various Reynolds numbers

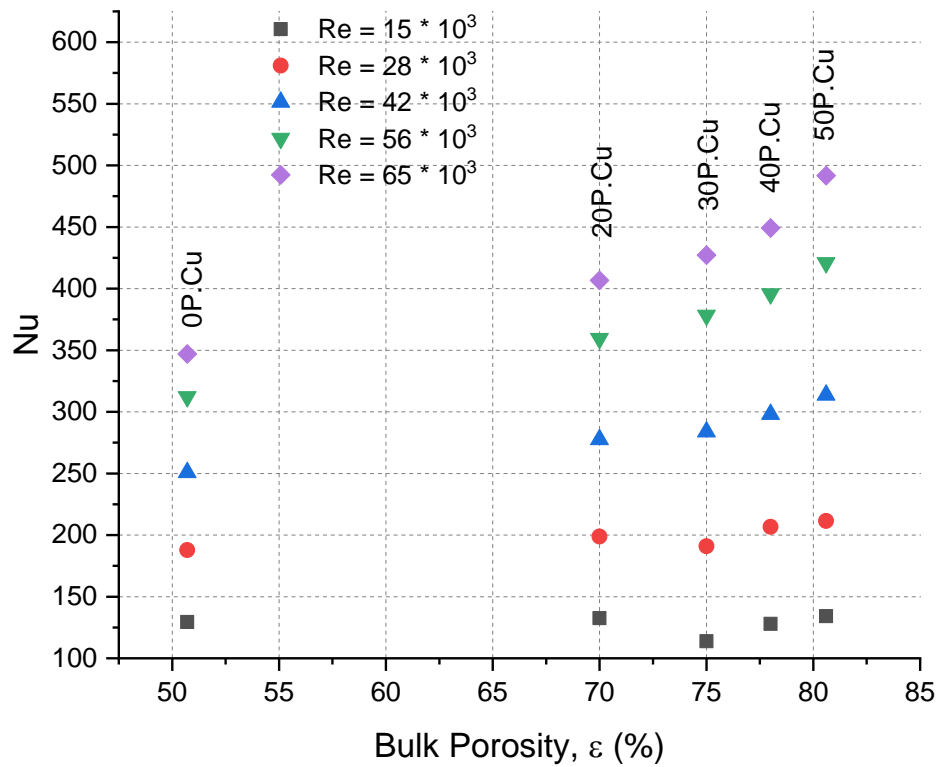


Figure 7. Nusselt number of path A against bulk porosity of porous sheets at various Reynolds numbers

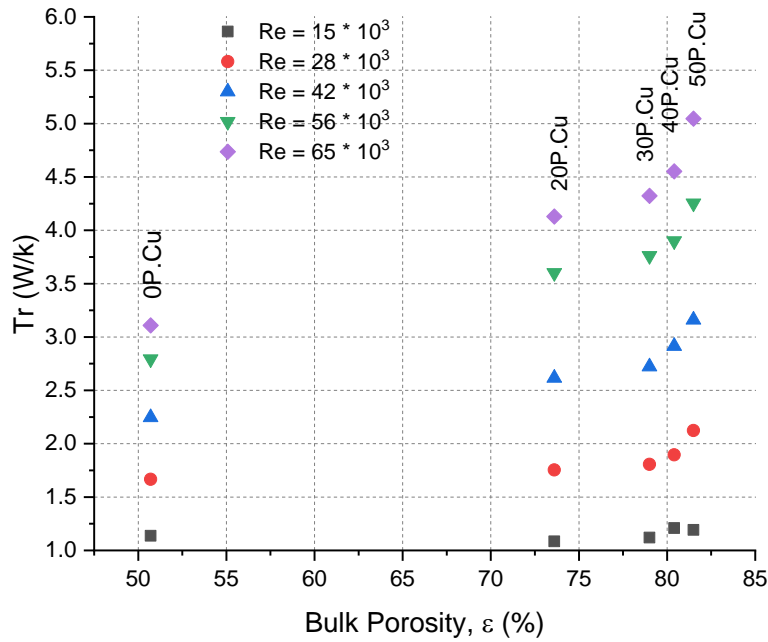


Figure 8. Thermal transmittance of path B against bulk porosity of porous sheets at various Reynolds numbers

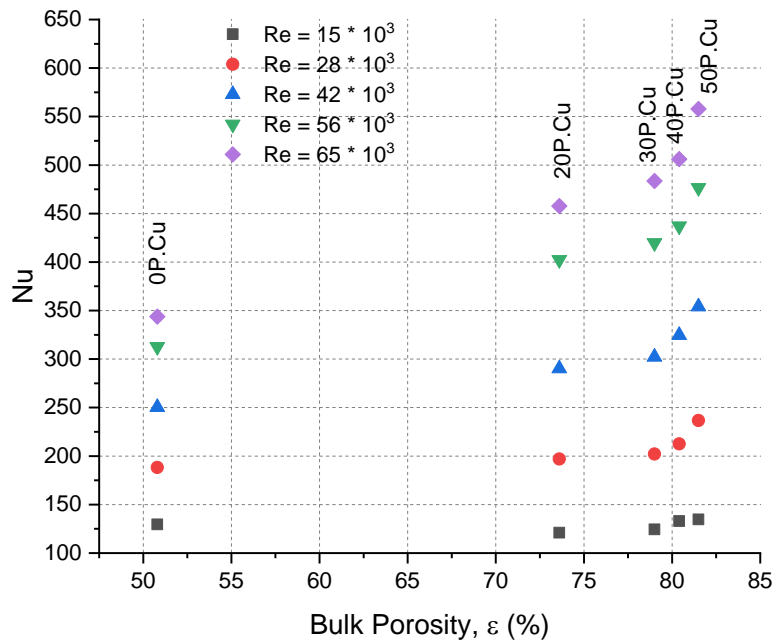


Figure 9. Nusselt number of path B against bulk porosity of porous sheets at various Reynolds numbers

Figure 6 shows the results of thermal transmittance for copper samples of path A plotted against the volumetric porosity at varying dimensionless Reynolds numbers. Figure 7 displays plots of the dimensionless Nusselt number against volumetric porosity at varying dimensionless Reynolds numbers for porous copper sheets of Path A. At lower Reynolds number regimes, a small change in the thermal transmittance and Nusselt number is achieved across a range of investigated porosities. At higher Reynolds number regimes, the change in the thermal transmittance and Nusselt number is clearer against porosity. 50P.Cu, which has the highest level of bulk porosity  $\epsilon = 81\%$ ,  $P_{Surt} = 60\%$  among the path A sheets, achieves thermal transmittance up to 4.37 W/K and Nusselt number 491.7. However, 0P.Cu, which has the lowest level of porosity, obtains the lowest thermal

transmittance ( $Tr$ ) of 3.08 W/K and Nusselt number 346.9, among the path A sheets. A similar trend is observed in path B porous sheets, as shown in Figures 8 and 9, which presents the plots of thermal transmittance and Nusselt number against volumetric porosity. 50P.Cu porous sheets with the highest rate of bulk porosity  $\varepsilon = 82\%$ ,  $P_{Surf}$  74% among the sheets of path B, obtains thermal transmittance and Nusselt number of 5.05 W/K and 557.9, respectively.

It is obvious from Figures 6 and 8 that the thermal transmittance may increase with the level of porosity in the porous sheets. The 50P.Cu porous sheet of path A has almost 38% higher thermal transmittance than that of the smooth sheet, and it is at least 28% higher when compared of a sheet with the lowest level of bulk porosity  $\varepsilon = 50.7$ . However, 50P.Cu of path B with  $\varepsilon = 82\%$  achieved a thermal transmittance that was approximately 53% better than that of the smooth sheet, also, it was 42% better compared to 0P.Cu with the lowest porosity. Moreover, it should be noted that the 0P.Cu has the lowest bulk porosity  $\varepsilon = 50.7\%$ ,  $P_{Surf} = 28\%$  among the porous samples for the both paths. the lowest thermal transmittance was gained with only increment of 10.7% of that from the smooth copper sheet.

The high thermal transmittance can be obtained at various samples of higher porosities. As mentioned earlier in Table 2, the thermal transmittance shows a clear dependency on the interaction of fluid dynamics of the active surface to the flow field [24]. Furthermore, the sheets with higher porosity show high active surface area and thermal transmittance. This could mean that the structure of samples has an important effect on the thermal performance of a system. Macropores and micropores have highly effect on the bulk porosity,  $\varepsilon$  and surface porosity,  $P_{Surf}$  of the current sheets. Numbers of macropores within the porous sample could improve the heat transfer performance better than numbers of micropores. The reason for this might be due to that the cooling fluids flow more easily through macropores than micropores. Due to this, the surface area resulting from the macropores can affect the active surface area through the sample to the cooling air better than the micropores [10]. Therefore, increasing the number of macropores could have high effect on the active surface area through a porous sample, thus improving the heat transfer capability. The deviations of the thermal transmittance for the tested samples of paths A and B for different volumetric porosities are shown in Figure 10. The deviations of the thermal transmittance can increase when the volumetric porosity also increase in paths A and B.

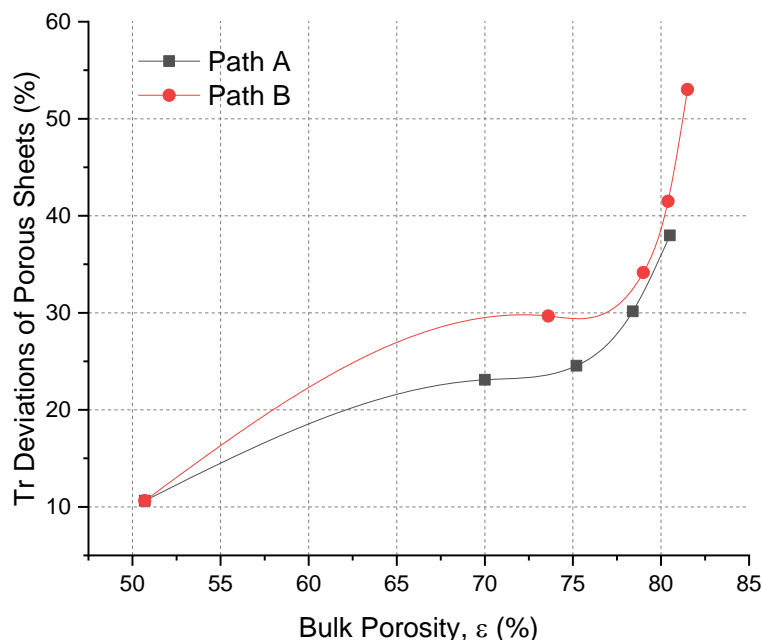


Figure 10. Plot of deviations of porous copper against volumetric porosity for paths A and B

In comparison, examining the two processing paths collectively, as shown in Figure 11, the sheets of path B have much higher thermal transmittance compared with sheets of path A. The porous sheets tested with the highest rate of porosity 82% with 50P.Cu of path B achieved a thermal transmittance of 53% better than the reference smooth sample in at high Reynolds number. However, the porous strips of path A achieve a thermal transmittance that is 38% better than the reference smooth sample.

The high porosities samples have wide active surface areas therefore they are estimated to achieve high thermal transmittance specially at high Reynolds numbers. Figure 6 and Figure 8 show the thermal transmittance of porous strips which it increases with an increase in porosity at high Reynolds numbers. The highly porous strips seem permeable to the cooling fluid, which is significant for the process of heat transfer. Moreover, porous strips could make the samples rougher than without them.

The roughness of the surface of the porous copper sheets was studied, as seen from Table 2. The porous sheets of path A, 0P.Cu demonstrates the lowest value of arithmetic average roughness,  $R_a = 0.03$  mm. Nevertheless, the 20P.Cu of path A shows  $R_a$  and number of peaks per centimeter length,  $m$  of 0.411 mm & 3.4 peak per centimeter, respectively. Additionally, 30P.Cu & 40P.Cu of path A could achieve Roughness of 0.88 mm & 0.96 mm and  $m$  of 4.3 & 4.6 peak per centimeter, respectively. The last sheet of 50P.Cu of path A declares an  $R_a$  of 1.2 mm and  $m$  of 4.86 peak per centimeter. Porous sheets of path B shows high similarity to the path A except the 50P.Cu of path B that records  $R_a$  and  $m$  of 1.0 mm and 5.4 peak/cm, respectively.

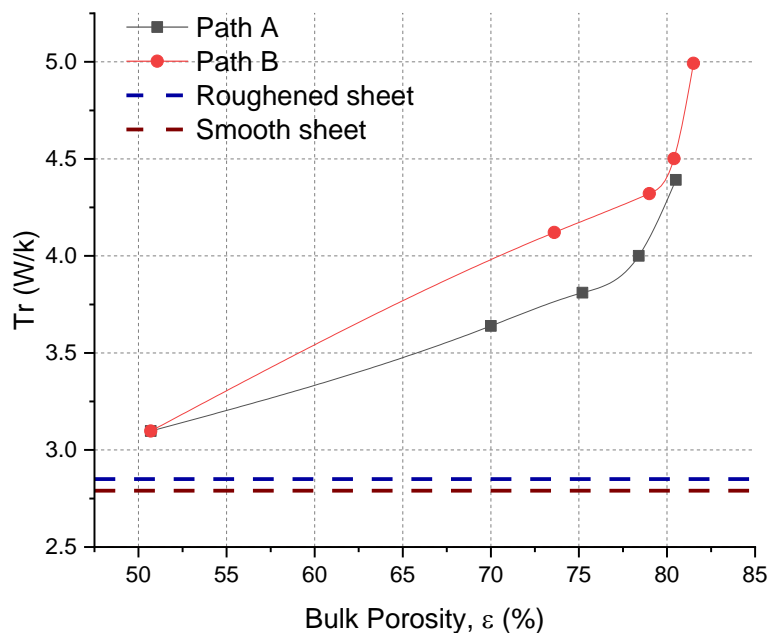


Figure 11. Comparison of the thermal transmittance of paths A and B against volumetric porosity at high Reynolds number of  $65 \times 10^3$

Uneven protrusions appear on the structure of the sample surface during the procedure due to the formation of copper powder. The surface roughness could stay even after removing bumps. The thermal transmittance can be affected by the produced surface roughness. Firstly, the fluid dynamic connection between the flow field and surface could be influenced by protrusions on the surface that may enhance convective heat transfer. Secondly, high thermal transmittance is expected to be gained when the uneven surface increases which could increase the convective heat transfer. Furthermore, the thermal transmittance could enhance to 1.2% at high Reynolds number due to roughening the smooth copper strip that could increase the surface area for the sheet., which marginally recovers the convection way of heat transfer.

Boundary layer conditions might be influenced by pore and pore wall morphology and also roughness of the surface, so that the convective heat transfer may also affected when it relies on that layer. Differences in the performance of heat transfer, however, may happen due to the flow manners around the source of heat.

The morphology of the surface of porous strips contents both porous and rough surface. So that the first section of the air was obliged to pass through the pores of the heat exchanger, while the other section was flown around the rough surface. The rate of heat transfer was high because of the increasing in surface area and also due to the existence of protrusions on the surface of the heat exchanger.

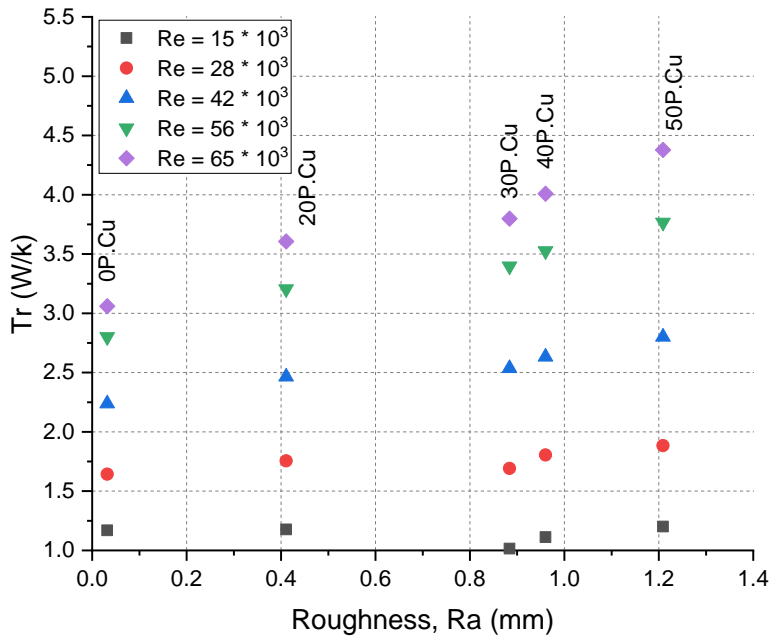


Figure 12. Experimental data of the performance of heat transfer against the surface roughness of porous sheets from path A

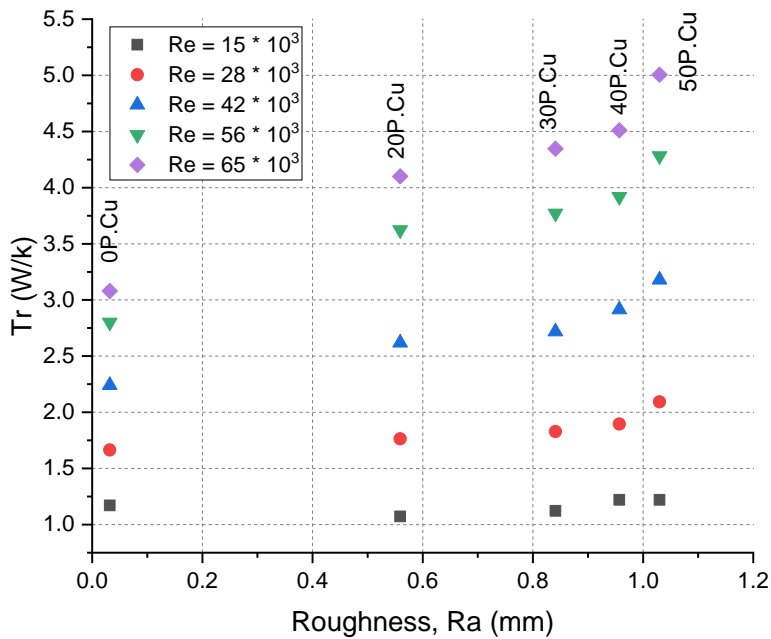


Figure 13. Experimental data of the performance of heat transfer against the surface roughness of porous sheets from path B

Back to Figure 3 and Figure 4, it can be seen that the CHF faces the cold air flow in the test section. This position could make the flow direction in prime with the sample which could pass a lot of cooling air into inlet and outlet of the current sheets, as seen in Figure 14. The rate of heat dissipation from the porous sheets increased through the boundary layer due to the mentioned position. In addition, the majority of the amount of air in the boundary

layer might flow over the rough surface of the tested samples, whereas the rest of the air could pass through the pores and channels.

Disturbances, which was due to air flow through the pores in the rough surface, was available in the boundary layer. As a result, a shrinkage of the boundary layer can be apparent. Moreover, a high rate of heat transfer was because of the profile of the velocity and temperature. Thin sheets, which were gained from the current work, could suit the process of improving heat transfer in such a constrained volume to mimic a high blockage ratio.

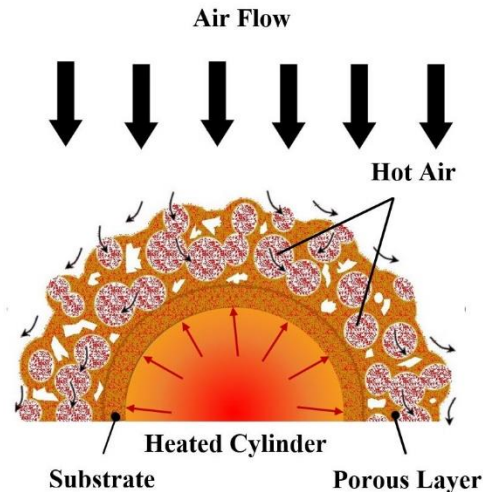


Figure 14. Diagram demonstrates the airflow in the face of the rough porous sheet

All in all, an increase in thermal transmittance can be seen from the current porous copper sheets. This increment was also from the increase in the roughness of surface. The porosity in surfaces of the current samples may enhance the convective heat transfer compared to dimpled surfaces. Furthermore, a noticeable enhancement in heat transfer can occur even in a reduced volume of a large porous.

#### 4. Conclusion

Double-layer, porous-dense copper sheets of thickness up to 1.4 mm were successfully fabricated by Lost Carbonate Sintering for casting copper strips, and their heat transfer performance was investigated. Smooth copper sheets were tested as references. The current study also reveals that porous layers with a bulk porosity ranges from 51% to 82%, can enhance the thermal transmittance. In path A, the produced porous strip with high porosity of up to 81% would increase the thermal transmittance by 38% in comparison to the smooth sheet under the same conditions. In path B, the produced porous sheets gained a thermal transmittance 53% higher than the smooth sheet. Surface porosity has a direct effect on the permeability of the porous samples, and therefore, it affects the thermal transmittance. When comparing the two paths, sheets from path B can accomplish higher thermal transmittance than the strips of path A because of a high porosity about 73.4% compared to sheets from path A could reach 60.5%. Both high porosities and surface roughness can contribute negatively or positively to heat transfer. The thermal transmittance increases up to the most porous sample tested, indicating that even higher porosities may increase performance still further, through there would be an upper limit encountered where the metal could no longer transport enough flux of heat. The porous strip had a potential impact on such structures that have thicknesses lower than 1.4 mm. Moreover, the capability of strips to be deformed all over the curved surfaces was exposed by the current investigation, which are still ongoing, and this behavior, therefore, testifies their functionality.

#### Acknowledgements

The authors would like to gratefully acknowledge the Department of Materials Engineering for financial support through Diyala University.

## Nomenclature

A	Surface Area
CHS	Cylindrical Heating System
D	Tested Cylindrical Diameter
h	Forced Convection Heat Transfer Coefficient
HWA	Hot Wire Anemometer
k	Thermal Conductivity of Air
Nu	Nusselt Number
P	Main Electrical Power
m	Number of peaks per unit length (in cm)
$P_{\text{Surf}}$	Surface Porosity
$Q_{\text{Cond}}$	Conduction Heat Transfer
$Q_{\text{Conv}}$	Convection Heat Transfer
$Q_{\text{Rad}}$	Radiation Heat Transfer
Ra	Roughness Value
Re	Reynolds Number
$T_a$	Free-Stream Temperature
$T_f$	Film Temperature
$T_r$	Thermal Transmittance
$T_s$	Surface Temperature
$T_t$	Temperature of The Wind Tunnel Walls
Greek Symbols	
$\varepsilon$	Volumetric of Bulk Porosity
$\epsilon$	Surface Emissivity
$\nu$	Kinematic Viscosity
$\sigma_B$	Stefan Boltzmann Constant
$\rho_a$	Apparent Density
$\rho_t$	True Density of The Porous Samples

## References

- [1] S.-S. Hsieh, R.-Y. Lee, J.-C. Shyu, and S.-W. Chen, "Thermal performance of flat vapor chamber heat spreader," *Energy Convers. Manag.*, vol. 49, no. 6, pp. 1774–1784, 2008.
- [2] T. Schubert, Ł. Ciupiński, W. Zieliński, A. Michalski, T. Weißgärber, and B. Kieback, "Interfacial characterization of Cu/diamond composites prepared by powder metallurgy for heat sink applications," *Scr. Mater.*, vol. 58, no. 4, pp. 263–266, 2008.
- [3] R. Goodall and A. Mortensen, "24 – Porous Metals," in *Physical Metallurgy*, 2014, pp. 2399–2595.
- [4] D. J. Thewsey and Y. Y. Zhao, "Thermal conductivity of porous copper manufactured by the lost carbonate sintering process," *Phys. Status Solidi Appl. Mater. Sci.*, vol. 205, no. 5, pp. 1126–1131, 2008.
- [5] Z. Xiao and Y. Zhao, "Heat transfer coefficient of porous copper with homogeneous and hybrid structures in active cooling," *J. Mater. Res.*, vol. 28, no. 17, pp. 2545–2553, 2013.
- [6] T. Ogushi, H. Chiba, and H. Nakajima, "Development of Lotus-Type Porous Copper Heat Sink," *Mater. Trans.*, vol. 47, no. 9, pp. 2240–2247, 2006.
- [7] H. F. Chen, Y. Liu, L. T. Chen, and Y. X. Li, "Heat Transfer Performance of Lotus-Type Porous Copper Micro-Channel Heat Sink," *Mater. Sci. Forum*, vol. 749, pp. 414–420, 2013.
- [8] K. Muramatsu, T. Ide, H. Nakajima, and J. K. Eaton, "Heat Transfer Performance of Lotus-Type Porous Metals," no. 44786. pp. 31–40, 2012.

- [9] H. Chiba, T. Ogushi, S. Ueno, and H. Nakajima, "Heat Transfer Capacity of Lotus-Type Porous Copper Heat Sink for Air Cooling," *J. Therm. Sci. Technol.*, vol. 5, no. 2, pp. 222–236, 2010.
- [10] L. Zhang, D. Mullen, K. Lynn, and Z. Yuyuan, "Heat Transfer Performance of Porous Copper Fabricated by the Lost Carbonate Sintering Process," *Mater. Res. Soc. Symp. Proc.*, vol. 1188, 2009.
- [11] S. Mancin, C. Zilio, A. Diani, and L. Rossetto, "Experimental air heat transfer and pressure drop through copper foams," *Exp. Therm. Fluid Sci.*, vol. 36, pp. 224–232, 2012.
- [12] P. M. Kamath, C. Balaji, and S. P. Venkateshan, "Convection heat transfer from aluminum and copper foams in a vertical channel - An experimental study," *Int. J. Therm. Sci.*, vol. 64, pp. 1–10, 2013.
- [13] G. Tomás, D. Martins, A. Cooper, and G. Bonfait, "Low-temperature thermal conductivity of highly porous copper," *IOP Conf. Ser. Mater. Sci. Eng.*, vol. 101, p. 012004, 2015.
- [14] G. J. Davies and S. Zhen, "Metallic foams: their production, properties and applications," *J. Mater. Sci.*, vol. 18, no. 7, pp. 1899–1911, 1983.
- [15] J. Banhart, "Manufacture, characterisation and application of cellular metals and metal foams," *Prog. Mater. Sci.*, vol. 46, no. 6, pp. 559–632, 2001.
- [16] B. L. Lefebvre, J. Banhart, and D. C. Dunand, "Porous Metals and Metallic Foams: Current Status and Recent Developments \*\*," vol. 10, no. 9, pp. 775–787, 2008.
- [17] V. C. Srivastava and K. L. Sahoo, "Processing, stabilization and applications of metallic foams. Art of science.," *Mater. Sci.*, vol. 25, no. 3, pp. 733–753, 2007.
- [18] H. Hermann, W. Pitschke, and N. Mattern, "Surface Roughness of Porous Materials and Its Characterization by X-Ray Absorption Measurements," *Phys. status solidi*, vol. 132, no. 1, pp. 103–114, 1992.
- [19] G. Kerckhofs, G. Pyka, M. Moesen, S. Van Bael, J. Schrooten, and M. Wevers, "High-Resolution Microfocus X-Ray Computed Tomography for 3D Surface Roughness Measurements of Additive Manufactured Porous Materials," *Adv. Eng. Mater.*, vol. 15, no. 3, pp. 153–158, 2013.
- [20] M. Rajczakowska, D. Stefaniuk, and M. Sobótka, "Roughness analysis of the 'invisible' surface by means of X-ray micro-CT," pp. 1–4.
- [21] Y. Y. Zhao, T. Fung, L. P. Zhang, and F. L. Zhang, "Lost carbonate sintering process for manufacturing metal foams," *Scr. Mater.*, vol. 52, no. 4, pp. 295–298, 2005.
- [22] J. Schindelin *et al.*, "Fiji: an open-source platform for biological-image analysis," *Nat Meth*, vol. 9, no. 7. Nature Publishing Group, a division of Macmillan Publishers Limited. All Rights Reserved., pp. 676–682, Jul-2012.
- [23] J. Schindelin, C. T. Rueden, M. C. Hiner, and K. W. Eliceiri, "The ImageJ ecosystem: An open platform for biomedical image analysis," *Mol. Reprod. Dev.*, vol. 82, no. 7–8, pp. 518–529, 2015.
- [24] L. Ventola, L. Scaltrito, S. Ferrero, G. Maccioni, E. Chiavazzo, and P. Asinari, "Micro-structured rough surfaces by laser etching for heat transfer enhancement on flush mounted heat sinks," *J. Phys. Conf. Ser.*, vol. 525, p. 012017, 2014.
- [25] "Versarien." [Online]. Available: <http://www.versarien-technologies.co.uk/>. [Accessed: 05-Aug-2018].